ISSN 1990-3413, Astrophysical Bulletin, 2023, Vol. 78, No. 3, pp. 293–303. © Pleiades Publishing, Ltd., 2023.
Original Russian Text © The Author(s), 2023, published in Astrofizicheskii Byulleten', 2023, Vol. 78, No. 3, pp. 305–315.

Gas Kinematics in the Magellanic-Type Galaxy NGC 7292

A. S. Gusev[1]*, A. V. Moiseev[1,2], and S. G. Zheltoukhov[1]**

[1]*Sternberg Astronomical Institute, Moscow State University, Moscow, 119234 Russia*
[2]*Special Astrophysical Observatory, Russian Academy of Sciences, Nizhnii Arkhyz, 369167 Russia*

Received April 22, 2023; revised June 5, 2023; accepted June 6, 2023

Abstract—he paper presents results of studying the kinematics of the ionized gas in the galaxy of the Large Magellanic Cloud type NGC 7292 obtained with the 2.5-m telescope of the Caucasian Mountain Observatory (CMO SAI MSU) and the 6-m BTA telescope of the Special Astrophysical Observatory (SAO RAS). Analysis of the velocity fields of the ionized and neutral hydrogen showed that the kinematic center of NGC 7292 located at the center of the bar, northwest of the photometric center of the galaxy (the southeastern end of the bar) previously taken as the center of NGC 7292. In addition to the circular rotation of the gas, the radial motions associated with the bar play a significant role in the kinematics of the disk. The observed perturbations of the gaseous-disk kinematics induced by the ongoing star formation do not exceed those caused by the bar. It is possible that part of the non-circular motions (at the southeastern end of the bar which is the brightest H II region) may be related to the effects of the capture of a dwarf companion or a gaseous cloud.

DOI: 10.1134/S1990341323700104

Key words: *galaxies: irregular—galaxies: evolution—interstellar medium: kinematics—galaxies: individual: NGC 7292*

1. INTRODUCTION

Disk galaxies of extremely late types of intermediate masses, the closest analogue of which is the Large Magellanic Cloud, are a relatively rare type of galaxies. Being, in most cases, of an asymmetric shape, they are the result of complex evolutionary processes: interactions with large neighbours or possible merging with companions (see, e.g., Zaritsky, 2009; Besla et al., 2012; Yozin and Bekki, 2014; Harris and Koch et al., 2015; Pardy et al., 2016; Siejkowski et al., 2018). One of these star systems is a nearby but relatively poorly-studied galaxy of the IBm type (according to the NED[1)] database) NGC 7292 (Fig. 1).

The galaxy is prominent with a heavy bar displaced from the disk. At the end of the bar, large star-forming regions are located, which are the brightest areas in the short-wavelength optical bands (U and B) and in the Hα line (Fig. 1). The southeastern part of the bar is usually taken as the galaxy's center (see, for example, the NED database), although, Gusev and Esipov (1996), based on multicolour surface photometry data, assumed that the center of the bar is the center of NGC 7292.

The parameters of the galaxy are determined quite reliably. According to the LEDA database[2)], its absolute magnitude $M(B)_0^i = -16.7 \pm 1.0$, the positional angle is 113°, and the inclination of the disk equals 54.°4. The bar, which suppresses the emission of a weaker disk, plays a decisive role in the calculation of the last two parameters. The distance to NGC 7292 also remains an open question (see the distance estimates in NED), while the radial velocity of the galaxy relative to the Sun (986 km s^{-1}) is determined quite reliably. We accepted the distance to the galaxy as $d = 6.82$ Mpc according to Tully et al. (2009) which corresponds to the 33 pc arcsec^{-1} scale. All the distance-dependent estimates taken from other papers (luminosity, sizes, etc.) are given precisely to this distance in our paper.

The galaxy NGC 7292 belongs to the NGC 7331 group but is located on its periphery and has no close companions (Ludwig et al., 2012).

The rotational curve of NGC 7292 was obtained in the paper by Esipov et al. (1991) from the [S II] emission lines. With an accepted disk inclination of 36°, the authors have found that the rotation velocity reaches 100 km s^{-1} at a distance of 800 pc from the center. However, in the specified paper, there

*E-mail: gusev@sai.msu.ru
**E-mail: moisav@gmail.com

1)http://ned.ipac.caltech.edu

2)http://leda.univ-lyon1.fr

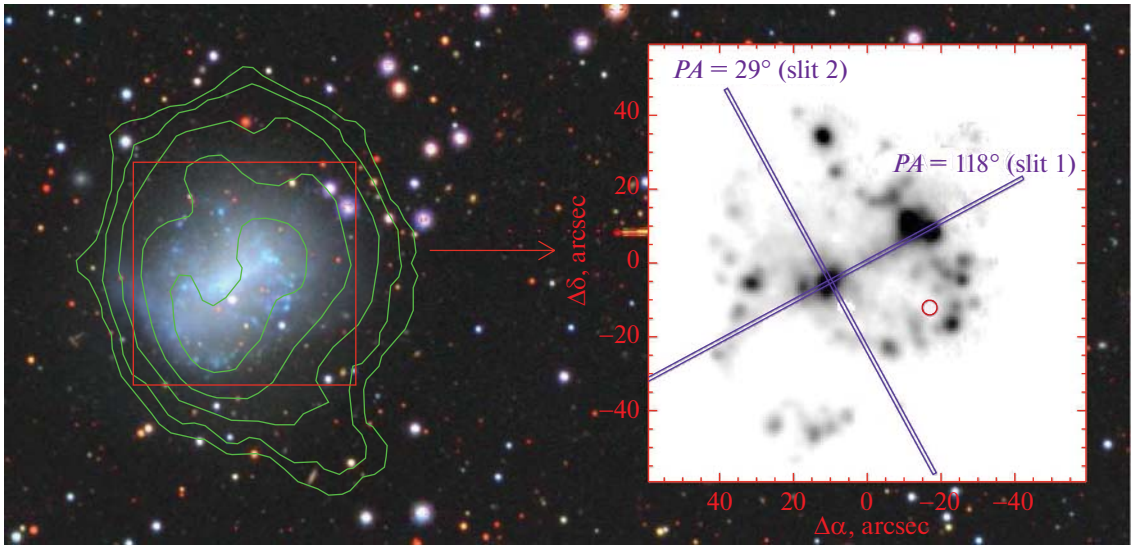

Fig. 1. Image of NGC 7292 from the DESI Legacy survey (Dey et al., 2019). The H I lines of equal density are shown in green according to Biswas et al. (2022). In the right-hand inset, the image in the Hα line obtained with the scanning FPI is given. We show the slit positions of the spectrograph. The center of coordinates corresponds to the nucleus of the galaxy. The red circle indicates the position of the supernova 1964H. North is on the top, East is on the left.

is no information on the kinematic center and the positional angle of NGC 7292 which does not allow one to verify the results obtained by Esipov et al. (1991).

Recent studies of the neutral hydrogen carried out with the Indian GMRT radio interferometer (Biswas et al., 2022) have shown that NGC 7292 has a regularly rotating disk H I of an approximate diameter of $3'$ (6 kpc) and a mass of $(2.08 \pm 0.06) \times 10^8\ M_\odot$ (at the H I column density level from 1×10^{20} cm^{-2} and higher). The authors give the "photometric" positional angle of the disk equal to 9°, however, the H I velocity field map indicates the kinematic positional angle $PA_{\rm kin} \approx 250°$.

The H I disk in NGC 7292 is round with the exception of a small protrusion on the southwestern outskirts (see Fig. 1). This protrusion does not differ from the major H I disk in velocity and velocity dispersion (Biswas et al., 2022, see details in Section 3). The observed asymmetric structure is morphologically similar to the part of the tidal tail which, together with the distorted shape of the outer optical isophotes, can be indicative of a relatively recent (less than 1–2 disk revolutions ago) event associated with the capture of the outer matter.

A large number of H II regions are observed in the galaxy (Gusev and Dodin, 2021). A supernova of type II (1964H) is known that burst in the western chain of H II regions (the J2000 coordinates: $\alpha = 22^{\rm h}28^{\rm m}24\overset{\rm s}{.}06$, $\delta = +30°17'23\overset{''}{.}3$; Crowther (2013)).

Spectroscopic observations with the bar-aligned long slit ($PA = 118\overset{\circ}{.}3$) carried out in the paper by Gusev and Dodin (2021) allowed one to estimate the chemical abundance of the gas in nine H II regions. It has been shown that the oxygen and nitrogen abundances in the H II regions are typical of galaxies of the specified luminosity (O/H $= 8.26 \pm 0.03\ dex$, N/H $= 6.86 \pm 0.07$ dex) with the absence of a radial metallicity gradient. A weak gradient of N/O was noticed along the bar major axis of NGC 7292: the N/O ratio is decreasing from the eastern to the western part of the galaxy.

Among the H II regions, a region in the bar center stands out (region C in Fig. 2), in which a low N/O ratio is observed; in the diagnostic diagram [N II]/Hα–[O III]/Hβ (Baldwin et al., 1981; Kewley et al., 2001; Kauffmann et al., 2003), it is located near the boundary separating objects with thermal and non-thermal (shock waves, ionizing emission from the active galactic nucleus) mechanism of excitation of emission lines (see Fig. 5 in the paper by Gusev and Dodin, 2021). In addition, the region at the center of the bar is characterized by the maximum O/H ratio in the galaxy. The brightest H II region located at the southeastern end of the bar (region A in Fig. 2) shows the maximum N/O value with the average O/H (Gusev and Dodin, 2021).

The spectrum of the galaxy obtained in the paper by Gusev and Dodin (2021) attracted attention due to the unusual rotation curve which served an incentive to studying the gas kinematics in NGC 7292 in detail.

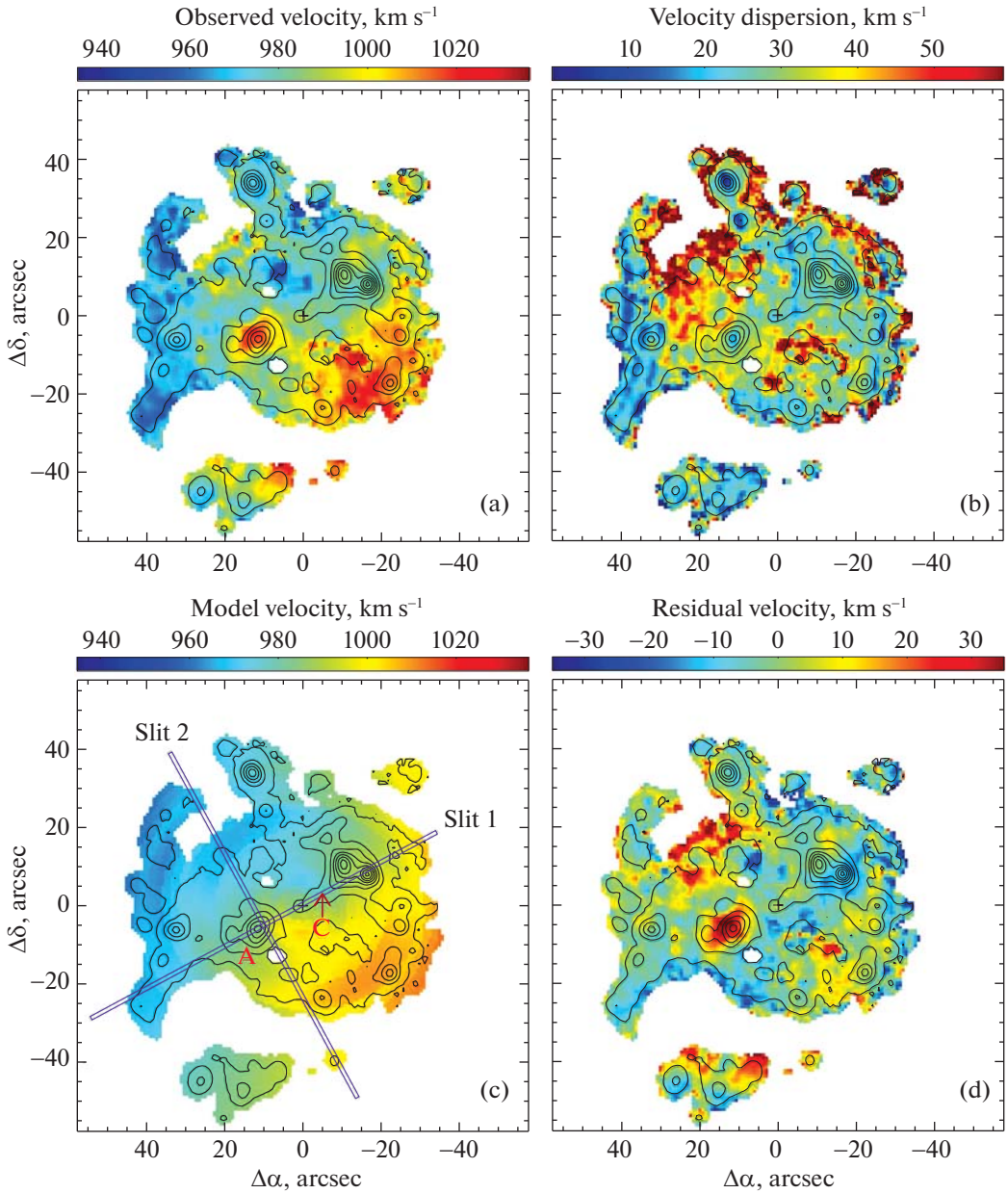

Fig. 2. Ionized-gas kinematics in the Hα line from the 6-m telescope data. The upper row shows the observed parameters: the radial velocity field (a) and the velocity dispersion field (b). The lower row shows the model velocity field (c) and the distribution of the deviation from the model (d). The cross in the maps marks the kinematic center of the galaxy. The arrow points the position of region C in the bar center. In the panel of the model velocity field, the positions of the spectrograph slits are indicated and two H II regions discussed in the text are marked.

2. OBSERVATIONS AND DATA REDUCTION

2.1. Panoramic Spectroscopy with the Fabry–Perot Interferometer

Observations of NGC 7292 with the scanning FPI installed in the SCORPIO multi-mode focal reducer (Afanasiev and Moiseev, 2011) were carried out with the 6-m SAO RAS telescope on October 9/10, 2021. The spectral range around the Hα line was separated with the $FWHM \approx 14$ Å narrow-band filter. During the observations, the gap between the plates of FPI was varied so that the obtained 40 interferograms uniformly filled the entire overlap-free spectral range $\Delta\lambda = 36$ Å). The exposure time was 90 s with the quality of stellar images being 1″.8–2″.8. The spectral resolution of FPI was 1.7 Å (which corresponded to 78 km s^{-1} at the Hα wavelength). The detector, the E2V 261-84 CCD camera, provided the field of view of about 6′.6 with a discretization of 0″.78/px in the readout mode with the 2 × 2 hardware binning.

Table 1. Observation log of CMO of SAI MSU

Slit	Date	T_{exp}, s	PA, deg	$\delta\lambda_{lab}$, Å
1	Dec 10/11, 2020	100+	118.3	2.53 ± 0.12
		3×900		
2a	May 01/02, 2021	900	−151.5	2.61 ± 0.19
2b	May 02/03, 2021	3×900	28.5	2.53 ± 0.14

After the primary reduction (a detailed description of the software used and references to original papers are given in Moiseev (2021)), the observations were presented as a data cube, in which each pixel in the field of view contained the spectrum of the region around the Hα line. The astrometric calibration was carried out online with `astrometry.net` (Lang et al., 2010). The resulting angular resolution after smoothing during the primary reduction was 2.″8.

The brightness distributions in the Hα emission, the radial velocity field in this line, and the field of the radial velocity dispersion free from instrumental broadening (Fig. 2) were constructed by approximating the spectra with the Voigt profile according to the method described in the paper by Moiseev and Egorov (2008).

2.2. Long-Slit Spectroscopic Observations

Observations were carried out with the 2.5-m telescope of the Caucasian Mountain Observatory of SAI MSU using the TDS transient two-beam spectrograph (TDS — the transient two-beam spectrograph). The spectrograph simultaneously operates in two channels: the blue (in the range of 3600–5770 Å with a dispersion of 1.21 Å/px, and a spectral resolution of 3.6 Å) and red (in the range of 5673–7460 Å, with a dispersion of 0.87 Å/px, and a spectral resolution of 2.6 Å). Two CCDs use the E2V 42-10 detectors of the size of 2048×512 px^2. The pixel size is 0.″363, the size of the used slits is $180'' \times 1''$. You can see the detailed description of the spectrograph the paper by Potanin et al. (2020).

The observations were carried out in December 2020 and May 2021 (see the observation log in Table 1) with the image quality of 1.″2–1.″8. During the first observation set, the slit was positioned along the bar of the galaxy ($PA = 118.^\circ3$), and during the second — perpendicular to the first ($PA = 28.^\circ5$), so that the slit passed through the brightest region of NGC 7292, the eastern end of the bar (see Fig. 1). During the observations in May, the slit in the second night (set 2b) was turned by 180° with respect to the first night (set 2a). The instrumental spectral line width ($FWHM$) $\delta\lambda_{lab}$, determined from the emission lines of the night sky, was 2.5–2.6 Å (115–120 km s^{-1}, see Table 1).

The observation procedure included obtaining the pflat fields and calibration images in the beginning and at the end of each observation series. Spectrophotometric standards were observed directly after the observations of the galaxy with the same air mass.

The original data was reduced according to the standard procedure including the dark-current correction, cosmic ray removal, flat-field correction, wavelength calibration using the Ne-Al-Si standard lamp and its correction with the night-sky lines, photometric calibration, adding the spectra of individual exposures, subtracting the background, and converting to the one-dimensional spectra (see the paper by Potanin et al. (2020) for detail). For the primary data reduction, we used the data reduction package based on `Python` developed in SAI MSU by A.V. Dodin; the further reduction was fulfilled with the `ESO-MIDAS system` for data reduction.

The radial velocity and velocity dispersion were determined from the wavelength and the Hα line width in 1″ increments. For this purpose, the spectrum was integrated within 1″, while the wavelength and the Hα line half-width (in the presence of emission) were determined by approximating the line with a Gaussian. The spectra were not corrected for the absorption component from the stellar population. As has been shown in the paper by Gusev and Dodin (2021), its contribution to the Hα lines is negligible: in all the H II regions studied, $EW(\mathrm{H}\alpha) > 40$ Å.

The observed radial velocity is reduced to heliocentric. The velocity dispersion σ was calculated taking into account the instrumental width $\delta\lambda_{lab}$: $\sigma^2 = \sigma^2_{obs} - \sigma^2_{lab}$, where $\sigma_{lab} = \delta\lambda_{lab}/(2\sqrt{2\ln 2})$, $\sigma_{obs} = \delta\lambda_{obs}/(2\sqrt{2\ln 2})$.

3. RESULTS

3.1. Radial Velocities and Velocity Dispersion of H II

The measurements of the radial velocities of the gas in the galaxy obtained using the long-slit spectroscopy and scanning FPI are consistent with each other within errors (Figs. 3 and 4). Both datasets show similar variations of the velocity dispersion along the slit, but the σ^2 measurements with the TDS are systematically higher than with the FPI, which is most likely due to two effects. First, the spectral resolution of the scanning FPI is one and a half times better, which is significant, since the observed line broadening due to the velocity dispersion is comparable to the width of the instrumental profile of the TDS ($\sigma_{lab} = 50 \pm 1$ km s^{-1}). Second, in the TDS

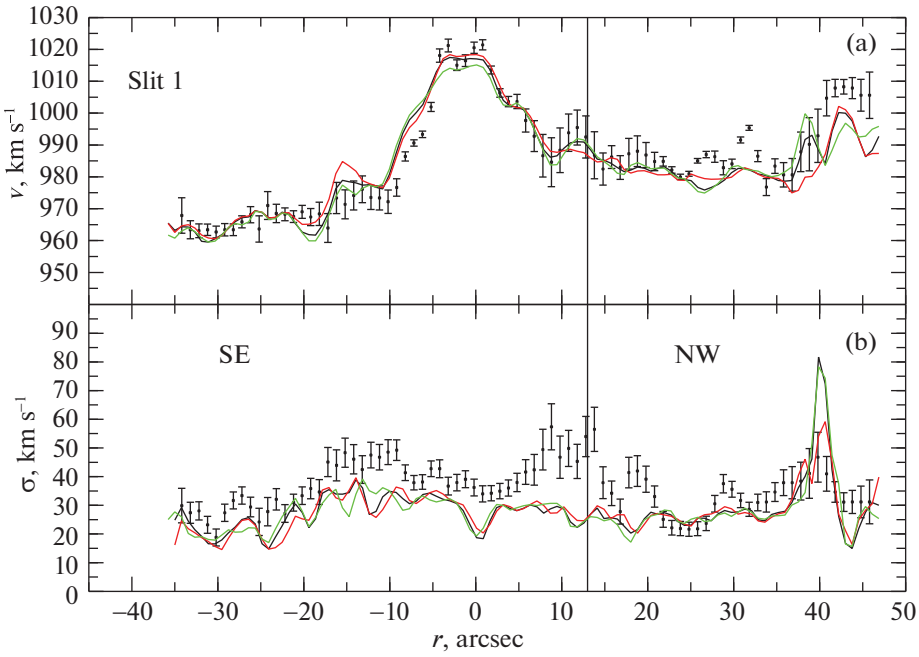

Fig. 3. Radial velocity (a) and velocity dispersion (b) of H II along the first slit position (PA = 118°28) according to the long-slit spectroscopy (the dots) and panoramic spectroscopy (the black curves). The red and green curves show the V and σ profiles obtained with the Fabry–Perot interferometer and right–left shifted relative to the slit by 1″. Measurement errors are shown. The center of the brightest H II region (the southeastern end of the bar, region A) is taken as the zero-point. The vertical line at $r = +13''$ corresponds to the kinematic center of the galaxy.

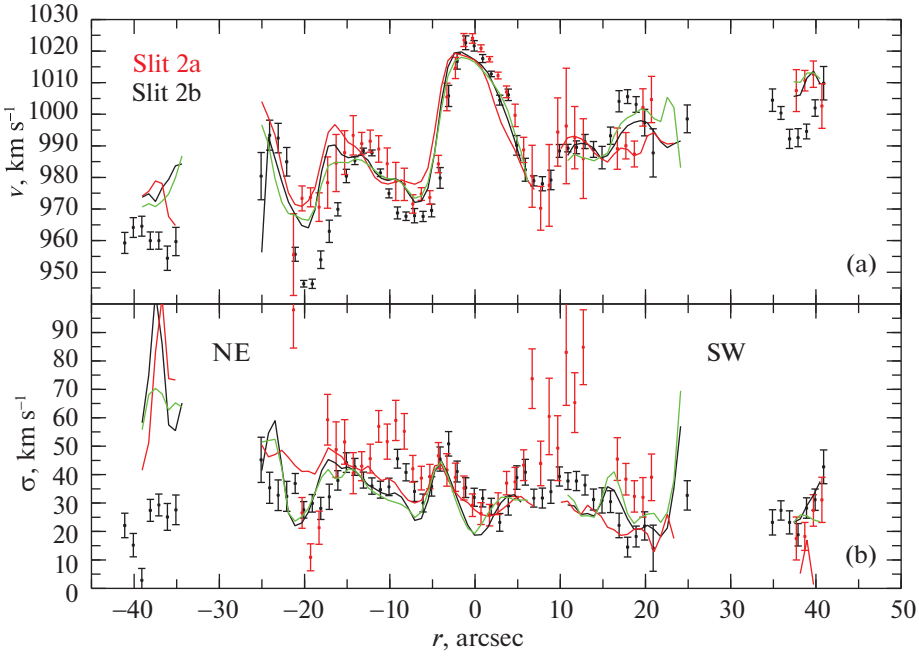

Fig. 4. Radial velocity (a) and velocity dispersion (b) of H II along the second slit position. The black dots show the position of 2b ($PA = 28°48$), the red dots—the position of 2a ($PA = -151°52$). Other designations are the same as in Fig. 3.

observations, the radial velocity distribution inside the slit is averaged, which also somewhat broadens the line profiles. So, in the top panels of Figs. 3 and 4, it is noticeable that the velocities determined from the velocity field constructed with the FPI by ΔV differ up to 5 km s^{-1} within 1″ (the black, red, and green curves).

The eastern end of the bar (the brightest H II region) with the velocity $V \approx 1020$ km s^{-1} stands out kinematically. The velocity along the rest of the

bar remains constant ($V = 980$–985 km s^{-1}). The velocity dispersion of the gas σ in the bar including its southeastern end is low, 20–40 km s^{-1}. It corresponds to the σ lower limit in NGC 7292 observed in some parts of the galaxy's disk. In the H II regions, σ does not exceed 30 km s^{-1} (Figs. 2–4). This value is slightly larger than that obtained by Law et al. (2022), $\sigma = 19 \pm 4$ km s^{-1}, for galaxies with the same star-formation rate (according to James et al. (2004), in NGC 7292 $SFR = 0.22 \pm 0.04\ M_\odot$ yr^{-1}), however, is consistent with the results by Moiseev et al. (2015) for galaxies of comparable luminosity in the visible range and Hα.

3.2. Parameters of the Disk Rotation from the Kinematics Data

To measure the rotation curve of a thin flat disk, it is necessary to find the following parameters that determine its orientation and kinematics: the position angle of the line of nodes (of the major axis) PA_0, the inclination of the disk to the line of sight i_0, the coordinates of the rotation center, and V_{SYS}, V_{ROT}—the systemic velocity and the rotation velocity. At the same time, with each specific radius, the kinematic position angle of the major axis PA_{kin} and the inclination of the orbits of gaseous clouds to the perspective plane i_{kin} may, for one reason or another, differ from PA_0 and i_0.

While PA_{kin}, and hence PA_0, is measured with confidence, as it characterizes the direction of the global radial velocity gradient, measuring the inclination angle i_0 is a problem. Analyzing the velocity field, one can conclude that this cannot be done, since the galaxy is in a position close to face-on ($i_0 < 40°$). The projected rotation velocity on the line of sight is not very large, while non-circular motions associated with the star-forming regions and gas flow in the bar make a very significant contribution to the observed situation. It is also difficult to establish the disk orientation from morphology, due to the fact that there is a strongly elongated bar in the inner part of the galaxy, and the outer regions are strongly perturbed (Figs. 1 and 5). Therefore, the position of the major axis along $PA_{kin} \approx 250°$ seen from the radial velocity fields of H I (see Section 1) and H II does not correspond to the major axis of optical isophotes (see Section 3.3) or distribution isodenses of H I. It is incorrect to determine the i_0 value from their ellipticity.

In order to estimate the disk inclination, we used the Tully–Fisher relation associating V_{ROT} with the luminosity of the galaxy. We used the tilted-ring method to determine the maximum rotation velocity by analyzing the H I velocity field provided by Biswas et al. (2022). The angular resolution of the H I data is $30'' \times 23''$, and the spectral one corresponds to 6.6 km s^{-1}. Let us note that the deviations from the circular rotation in the southwestern protrusion of the H I disk do not exceed 5 km s^{-1} which is even smaller than those in some internal regions of the H I disk. The neutral gas disk is longer and the maximum in the rotation curve can be found at $r = 60''$, where the ionized gas is no more observed. If we accept $M(B) = -16.7 \pm 1.0$ according to LEDA, from the calibration relations given in Rhee and Broeils (2005) for their RC sample, we obtain the supposed rotation curve amplitude 63 km s^{-1}. Fitting the radial velocity field using the tilted-ring model with different i_0 values showed that the required rotation velocities are achieved at $i_0 = 29° \pm 4°$.

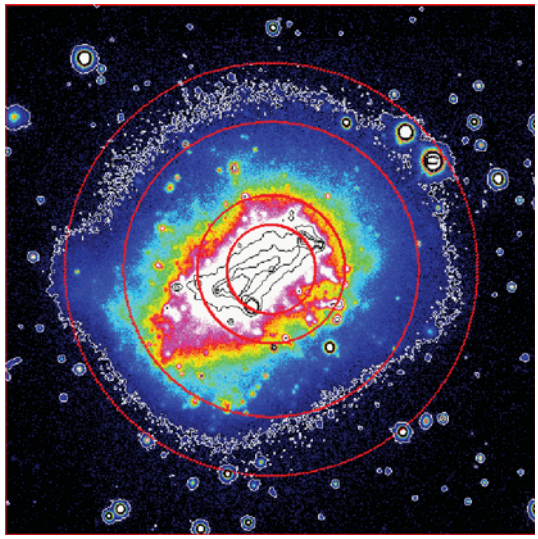

Fig. 5. Deep image of NGC 7292 in the r band of the Legacy Surveys before subtraction of the field stars. The radii of the circles are equal to $15''$, $25''$, $50''$, and $70''$. The external isophote given in white colour in r corresponds to the level of $3\,\sigma$ higher than the sky background.

The galactic disk rotation parameters were determined with the tilted-ring method adapted for analyzing the radial velocity field of the ionized gas (the detailed description and main ratios are given in the papers by Moiseev (2014, 2021). According to the accepted parameters of the outer disk orientation PA_0, i_0, the velocity field was divided into narrow elliptical rings, the radial velocity distribution in each ring of the radius r was fitted with a circular rotation model with the following parameters: V_{SYS}, V_{ROT}, PA_{kin}, and i_{kin}. The center of rotation, determined from considerations of field radial velocity symmetry, coincides within error with a small H II region at the center of the bar (region 5 from Gusev and Dodin (2021) located by $3\farcs5$ southeast of region C), therefore, in further analysis, it was fixed at this point with the coordinates $\alpha(\mathrm{J2000.0}) = 22^{\mathrm{h}}28^{\mathrm{m}}25\overset{\mathrm{s}}{.}34$, $\delta(\mathrm{J2000.0}) = +30°17'35\farcs3$. The mea-

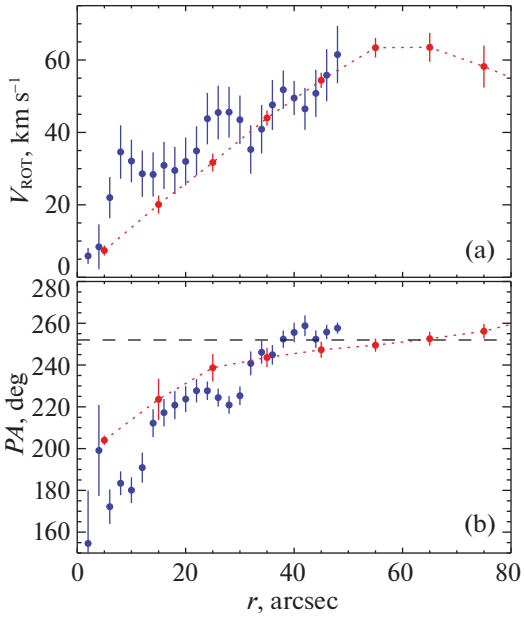

Fig. 6. Parameters of the kinematic model: the ionized-gas rotation curve (a) and the radial variations PA_{kin} (b). The blue symbols show the ionized gas, the red mark the neutral hydrogen. The black dashed line shows the accepted orientation of the line of nodes of the gaseous disk.

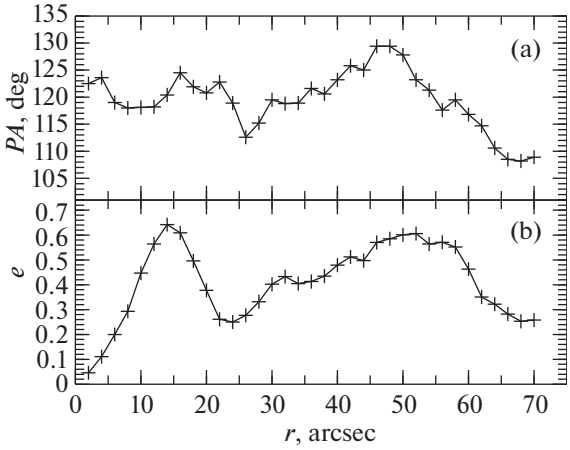

Fig. 7. Radial profiles of the position angle PA and ellipticity e obtained for the image of NGC 7292 in the r band.

surement accuracy of the kinematic center position is approximately $\pm 1''$. Moving the accepted position of the kinematic center to a greater distance (for example, to region C described in the Introduction and located at $3''.5$ from the chosen center) leads to noticeable (more than 10–15 km s^{-1}) variations in the systemic velocity along the radius, which are absent in the case of the rotation center we have adopted. Later, to obtain a more stable rotation model, the systemic velocity was fixed at the average value $V_{SYS} = 988 \pm 1$ km s^{-1}.

The radial variations in the gas rotation parameters in the galaxy are shown in Fig. 6. The orientation of the line of nodes defined as the average value of PA_{kin} at $r = 35''$–$45''$ is $PA_0 = 253 \pm 2°$. The rotation of the kinematic axis in the more internal regions of the galaxy is obviously associated with radial gas flows under the influence of the triaxial potential of the bar. The direct evidence here is the fact that the deviations of PA_{kin} from PA_0 occur in the opposite direction relative to the turn of the inner isophotes, whose major axis in the bar region is located along $PA \approx 305°$ (125°); while in the outer regions, the isophotes gradually turn closer to the accepted PA_0 value (Figs. 6 and 7). A detailed discussion of the technique for comparing photometric and kinematic PA in barred galaxies and references to the original papers are given in the review by Moiseev (2021); a comparison with the results of numerical simulations is presented, for example, in the paper by Moiseev and Mustsevoi (2000).

Figure 6 also shows the results of applying the same rotation model to the velocity field in H I from Biswas et al. (2022). One can see a fairly good agreement between the kinematics of the ionized and neutral hydrogen taking into account the fact that the angular resolution in the 21-cm line is an order of magnitude lower and amounts to $30'' \times 23''$. Thus, measurements of PA_{kin} and V_{ROT} in the Hα line within $r < 30''$ are sharper. The slow increase of PA_{kin} in H I for $r > 40''$ is possibly indicative of the bending of the outer gaseous disk, in which the ionized gas is almost no longer observed.

3.3. Photometric Parameters of the Disk

For comparison, using the data on the coordinates of the kinematic center of NGC 7292 and the image of the galaxy in the r band from the Legacy Surveys (Fig. 5), we present the obtained radial distribution of the photometric position angles PA and the isophote ellipticity $e \equiv 1 - b/a$ (Fig. 7). The parameters PA and e were calculated using the `SURFPHOT` software package in the `MIDAS` environment. The field stars were previously removed from the image shown in Fig. 5. The star-forming regions (the H II ones) of the galaxy were not subtracted from the image. As can be clearly seen from Figs. 5 and 7, they make a significant contribution at galactocentric distances $r < 30$–$35''$ without affecting the determination of the parameters for the outer-disk regions of NGC 7292.

Figure 7 shows a complex structure of NGC 7292. In the bar region ($r < 15''$), the ellipticity increase

from 0.05 to 0.65 is observed at the constant position angle ($PA = 118°-123°$). In the range of $r = 15''-25''$, the ellipticity drops sharply to 0.3 and the position angle decreases to 113°. This region corresponds to the brightest area of the disk actively emitting in the Hα line and limited by the chains of H II regions (see galaxy images in Figs. 1, 2, and 5). In the range of the galactocentric distances of $25''-50''$, a disk of moderate brightness can be observed with its symmetry center displaced relative to the kinematic center of NGC 7292 and located near the southeast end of the bar of the galaxy (Fig. 5). In this region, the isophote position angle reaches the maximum at 129.°5, and the ellipticity increases to 0.6. Both parameters, PA and e, at $r = 50''$ are close to the values obtained for $r = 15''$. Finally, in the outermost part of the galaxy, at $r = 70''$ (2.3 kpc), the ellipticity and position angle again decrease to the values close to those obtained at $r = 25''$ (Fig. 7).

As can be clearly seen, the parameters PA and e determined from the photometric data do not agree with those obtained from the velocity field analysis.

4. DISCUSSION

Figures 2c and 2d show the velocity field in the circular rotation model (more precisely, quasi-circular, since $PA_{\rm kin}$ varies with r) and residual velocities $V_{\rm res}$ after subtracting the model from observations. There are several features in their distribution. First of all, these are high moduli of $V_{\rm res}$ in two giant star-forming regions at the ends of the bar. This symmetric arrangement may be due to the fact that the residual velocities are associated with non-circular (usually, radial) movements in the bar, which are not fully accounted for by our quasi-circular rotation model. But it is strange that the amplitude of velocities in the regions symmetrical with respect to the center differs by a factor of two: $V_{\rm res}$ is $-10... - 15$ km s^{-1} in the northwestern but reaches $+30... + 37$ km s^{-1} in the southeastern region (region A). Then the velocity of the radial motions will be, in terms of the disk plane, $V_{\rm res}/\sin i = 23-35$ km s^{-1} and $71-87$ km s^{-1}, respectively. And if the first estimate looks reasonable, in the second case the velocity of the gas flow to the center exceeds the hyperbolic one at the given radius ($V_{\rm ROT} \approx 30$ km s^{-1} at $r = 20''$, Fig. 6) which is doubtful.

It is possible that such high peculiar velocities in the southeastern region designated as A (see Fig. 2) are not related to the radial direction but to some other, for example, to the vertical motions of the gas in the disk. The gas outflows from the star-forming regions associated with the gaseous envelope expanding under the action of supernova outbursts and stellar winds could be the most obvious reason. But in this case, it is not clear why we observe only the moving-away part of the envelope ($V_{\rm res} > 0$) and not the one expanding towards the observer. Moreover, the velocity dispersion map in the Hα line (Fig. 2), which is consistent with the long-slit spectroscopy data (Fig. 3), shows a pattern typical of dwarf galaxies with the ongoing star formation (Moiseev and Lozinskaya, 2012), namely: σ has minimum values at the centers of the bright H II regions, since here the main emission comes from denser gaseous clouds. At the same time, σ is higher on their periphery, since here we can see the emission of the diffuse gas which is more sensitive to the star-formation perturbation. If large values of $V_{\rm res}$ in the southeastern region were associated, for example, with a breakthrough of the expanding gas envelope, then it would be expected to observe a peak in the velocity dispersion. But this is not observed.

A typical situation associated with the interstellar medium perturbation caused by the star formation is observed along the major axis of the galaxy in the southwestern and northeastern parts of the disk, where regions of high σ have a low brightness in the Hα line and relatively high values of $V_{\rm res}$. At the same time, at least some of the non-circular gas motions near the large star-forming complexes is most likely associated with the tidal perturbation of the disk after the last interaction. Is it possible that the area southeast of the center is part of a companion that merged with NGC 7292? According to Gusev and Dodin (2021), this complex has the lowest internal extinction of all the studied H II regions in NGC 7292 determined from the Balmer decrement. This may testify in favor of the assumption that it enters the gaseous disk of the galaxy from the side of an observer from the Earth. On the other hand, the star-formation complex does not stand out by the oxygen abundance (its O/H $= 8.26 \pm 0.05$ dex corresponds to the average of the galaxy), and the position of the complex in the characteristic diagrams does not indicate the presence of the H II shock excitation mechanisms (Gusev and Dodin, 2021). Thus, the currently available observed data do not allow one to unambiguously identify the structures associated with a companion that has been swallowed up by the main galaxy.

This complex is at an evolutionally advanced stage of the star formation. Its N/O ratio is the highest among all the studied H II regions (Gusev and Dodin, 2021) and indicates the enrichment of the surrounding interstellar medium with nitrogen of secondary origin. The morphology of the complex also evidences the decrease (termination within the model of a single starburst) of the star-formation rate in the modern

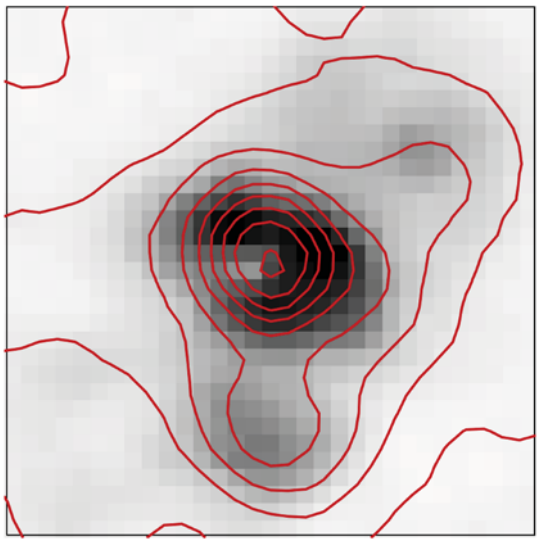

Fig. 8. Image of the brightest H II region of NGC 7292 (region A at the southeastern end of the bar) in the Hα + [N II] line with the superimposed isophotes in the U band. The image size is $8'' \times 8''$ (260 pc). North is on the top, East is on the left. We used the unpublished U data obtained with the 1.5-m telescope of the Maydanak Observatory (Uzbekistan), and in the Hα + [N II] line with the continuum subtracted obtained with the 2.5-m telescope of the CMO SAI MSU from the personal archive of one of the authors. The observations in the continuum (the filter with $\lambda_{\text{eff}} = 6427$ Å, $\Delta\lambda = 122$ Å) were carried out together with the observations in the Hα + [N II] line.

age. Figure 8 clearly shows that the Hα-emission region forms a ring of a diameter of 50–80 pc surrounding the star complex. According to Whitmore et al. (2011), this stage of evolution ("young cluster") occurs approximately 6–8 Myr after the starburst, when the first supernovae sweep out the gas to the periphery of the star complex. Note the asymmetry of the H II envelope: the maximum Hα emission is observed to the west (from the side of the bar) of the complex, where the gas density is apparently the highest.

If we assume that the star formation in this region is stimulated by an infall of a companion (gaseous or stellar-gaseous), then it should have occurred relatively recently, on time scales of about 10 Myr ago. This is indicated by: the age of the stellar population of complex A; the spatial scale of perturbations of the gaseous disk of NGC 7292 (the region of abrupt changes in radial velocities from 1020 to 980 km s^{-1} is $5''$–$8''$ (Figs. 2–4) which corresponds to the same time scale of 7–8 Myr with the observed $\sigma \approx 30$ km s^{-1} in this region); the distance traveled by a possible companion with the projected radial velocity relative to the galaxy equal to 40 km s^{-1}, for a time of 6–8 Myr, in order of magnitude, the effective thickness of the NGC 7292 disk is about 200 pc.

From the available data, we cannot say whether this local perturbation (a possible infall of a companion) is associated to longer-lived in time and larger-scale in distance evidence of tidal perturbations such as the bending of the H I outer disk beyond the optical radius, the asymmetry in the H I distribution, and the distorted shape of the external optical isophotes, or it is independent.

The galaxy has not previously been studied kinematically in detail. The newly observed data we have obtained show the peculiar, very difficult to interpret features of gas motion in the disk of NGC 7292. Having considered all possible cases above, we believe that the most realistic way to explain the radial velocity anomaly at the southeastern end of the bar (the brightest H II region in the galaxy previously taken as its center) is the infall of an outer companion.

5. CONCLUSION

The analysis of the velocity fields of the ionized and neutral hydrogen showed that the kinematic center of NGC 7292 is located at the center of the bar, northwest of the photometric center of the galaxy (the southeastern end of the bar) which has been previously taken as the center of NGC 7292. In addition to the circular rotation, the radial motions associated with the bar play a significant role in the kinematics of the gaseous disk. Compared to these non-circular motions, the observed perturbation of the gaseous disk by the star formation is not so strong: the differences from the circular rotation in the H II regions do not exceed those caused by the radial flows in the bar, and the velocity dispersion increases only in the diffuse ionized gas closer to the disk periphery. The velocity dispersion distribution does not contain any envelope structures characteristic of a number of dwarf galaxies with a starburst (Moiseev and Lozinskaya, 2012; Gerasimov et al., 2022). It is possible that some of the non-circular motions (primarily at the southeastern end of the bar—the brightest H II region) may be associated with the consequences of a merger with a dwarf companion or the capture of an external gaseous cloud. However, so far we have not managed to find direct evidence of this interaction. The presence of tidal perturbations, such as the bending of the outer H I disk beyond the optical radius, the asymmetry in the neutral hydrogen distribution, and the distorted shape of the outer optical isophotes, can be related to a possible infall of a companion at the southeastern end of the bar, or independent of it.

ACKNOWLEDGMENTS

The authors are grateful to the reviewer for valuable and useful comments. We thank E.I. Shablovinskaya and E.A. Malygin, who carried out observations with the 6-m SAO RAS telescope, A.V. Dodin, who did the primary reduction of the long-slit spectroscopy data, and Prerana Biswas, who kindly provided the H I maps obtained with the GWRT telescope. The open data of the HyperLEDA database (`http://leda.univ-lyon1.fr`) and NASA/IPAC Extragalactic Database (`http://ned.ipac.caltech.edu`) were used in the paper. We used the public data from the Legacy Survey (`http://legacysurvey.org`) consisting of three separate and complementary projects: the Dark Energy Camera Legacy Survey (DECaLS; Proposal ID ♯2014B–0404; PIs: David Schlegel and Arjun Dey), the Beijing-Arizona Sky Survey (BASS; NOAO Prop. ID ♯2015A–0801; PIs: Zhou Xu and Xiaohui Fan), and the Mayall z-band Legacy Survey (MzLS; Prop. ID ♯2016A–0453; PI: Arjun Dey). DECaLS, BASS, and MzLS together include the data obtained, respectively, with the Blanco telescope, Cerro Tololo Inter-American Observatory, NSF's NOIRLab; the Bok telescope, Steward Observatory, University of Arizona; and the Mayall telescope, Kitt Peak National Observatory, NOIRLab. The Project Legacy Survey was honored to receive permission to perform the astronomical research on Iolkam Duág (Kitt Peak), a mountain of special significance to the Tohono Oódham people.

FUNDING

The spectroscopic observations at the Caucasian Mountain Observatory of SAI MSU and the analysis of the long-slit spectroscopy data were supported by the RFBR grant No. 20-12-00080 and by the Interdisciplinary Scientific and Educational School of the Lomonosov Moscow State University "Fundamental and Applied Space Research". The observed data were partially obtained with the 2.5-m telescope of the Caucasian Mountain Observatory of SAI MSU. The development of the instrumental base of the observatory is carried out with the support of the Development Program of the Lomonosov Moscow State University. Observations with the 6-m SAO RAS telescope are supported by the Ministry of Science and Higher Education of the Russian Federation. The renovation of the instrumental base is carried out within the framework of the "Science and Universities" national project. The analysis of the ionized gas kinematics was carried out within the framework of the state assignment of SAO RAS approved by the Ministry of Science and Higher Education of the Russian Federation.

CONFLICT OF INTEREST

The authors declare no conflict of interest regarding the publication of this paper.

REFERENCES

1. V. L. Afanasiev and A. V. Moiseev, Baltic Astronomy **20**, 363 (2011).
2. J. A. Baldwin, M. M. Phillips, and R. Terlevich, Publ. Astron. Soc. Pacific **93**, 5 (1981).
3. G. Besla, N. Kallivayalil, L. Hernquist, et al., Monthly Notices Royal Astron. Soc. **421** (3), 2109 (2012).
4. P. Biswas, N. N. Patra, N. Roy, and M. Rashid, Monthly Notices Royal Astron. Soc. **513** (1), 168 (2022).
5. P. A. Crowther, Monthly Notices Royal Astron. Soc. **428** (3), 1927 (2013).
6. A. Dey, D. J. Schlegel, D. Lang, et al., Astron. J. **157** (5), article id. 168 (2019).
7. V. F. Esipov, G. A. Kyazumov, and A. R. Dzhafarov, Soviet Astronomy **35** (5), 452 (1991).
8. I. S. Gerasimov, O. V. Egorov, T. A. Lozinskaya, et al., Monthly Notices Royal Astron. Soc. **517** (4), 4968 (2022).
9. A. S. Gusev and A. V. Dodin, Monthly Notices Royal Astron. Soc. **505** (2), 2009 (2021).
10. A. S. Gusev and V. F. Esipov, Astronomy Reports **40** (3), 319 (1996).
11. J. Harris and D. Zaritsky, Astron. J. **138** (5), 1243 (2009).
12. P. A. James, N. S. Shane, J. E. Beckman, et al., Astron. and Astrophys. **414**, 23 (2004).
13. G. Kauffmann, T. M. Heckman, C. Tremonti, et al., Monthly Notices Royal Astron. Soc. **346** (4), 1055 (2003).
14. L. J. Kewley, M. A. Dopita, R. S. Sutherland, et al., Astrophys. J. **556** (1), 121 (2001).
15. A. Koch, M. J. Frank, A. Pasquali, et al., Astrophys. J. **815** (2), article id. A105 (2015).
16. D. Lang, D. W. Hogg, K. Mierle, et al., Astron. J. **139** (5), 1782 (2010).
17. D. R. Law, F. Belfiore, M. A. Bershady, et al., Astrophys. J. **928** (1), id. A58 (2022).
18. J. Ludwig, A. Pasquali, E. K. Grebel, and I. Gallagher, John S., Astron. J. **144** (6), article id. A190 (2012).
19. A. V. Moiseev, Astrophysical Bulletin **69** (1), 1 (2014).
20. A. V. Moiseev, Astrophysical Bulletin **76** (3), 316 (2021).
21. A. V. Moiseev and O. V. Egorov, Astrophysical Bulletin **63** (2), 181 (2008).
22. A. V. Moiseev and T. A. Lozinskaya, Monthly Notices Royal Astron. Soc. **423** (2), 1831 (2012).

23. A. V. Moiseev and V. V. Mustsevoi, Astronomy Letters **26**, 565 (2000).
24. A. V. Moiseev, A. V. Tikhonov, and A. Klypin, Monthly Notices Royal Astron. Soc. **449** (4), 3568 (2015).
25. S. A. Pardy, E. D'Onghia, E. Athanassoula, et al., Astrophys. J. **827** (2), article id. A149 (2016).
26. S. A. Potanin, A. A. Belinski, A. V. Dodin, et al., Astronomy Letters **46** (12), 836 (2020).
27. M.-H. Rhee and A. H. Broeils, J. Astron. and Space Sci. **22** (2), 89 (2005).
28. H. Siejkowski, M. Soida, and K. T. Chyży, Astron. and Astrophys. **611**, id. A7 (2018).
29. R. B. Tully, L. Rizzi, E. J. Shaya, et al., Astron. J. **138** (2), 323 (2009).
30. B. C. Whitmore, R. Chandar, H. Kim, et al., Astrophys. J. **729** (2), article id. A78 (2011).
31. C. Yozin and K. Bekki, Monthly Notices Royal Astron. Soc. **439** (2), 1948 (2014).

Translated by N. Oborina